JACS
JOURNAL OF THE AMERICAN CHEMICAL SOCIETY
Article
pubs.acs.org/JACS

Multimodal Shape Transformation of Dual-Responsive DNA Block Copolymers

Chan-Jin Kim, Xiaole Hu, and So-Jung Park*

Department of Chemistry and Nano Science, Ewha Womans University, 52 Ewhayeodae-gil, Seodaemun-gu, Seoul 120-750, Korea

Supporting Information

ABSTRACT: Herein, we report the self-assembly and multimodal shape transformation of dual-responsive DNA di- and triblock copolymers. Dual-responsive DNA diblock copolymer was synthesized by coupling a thermoresponsive polymer, poly(*N*-isopropylacrylamide (PNIPAM), and an oligonucleotide. DNA-*b*-PNIPAM possesses thermoresponsive properties of PNIPAM as well as molecular recognition properties of DNA. Thus, they undergo reversible temperature-triggered transition at lower critical solution temperature (LCST) between molecular DNA and polymer micelles with high density DNA corona. The hybridization of DNA-*b*-PNIPAM and DNA-modified nanoparticles generates functional nanoparticles showing unique temperature-dependent aggregation and disaggregation behaviors due to the dual-responsive nature of DNA-*b*-PNIPAM. DNA triblock copolymers of DNA-*b*-PNIPAM-*b*-PMA were synthesized by introducing a hydrophobic block, poly(methyl acrylate) (PMA), to DNA/PNIPAM block copolymers, which form spherical micelles at room temperature. They are capable of nanoscale shape transformation through the combination of thermal trigger and DNA binding. DNA-*b*-PNIPAM-*b*-PMA micelles undergo sphere-to-cylinder shape changes above LCST due to the conformational change of PNIPAM. The shape change is reversible, and fast cylinder-to-sphere transition occurs when the temperature is lowered below LCST. The low temperature spherical morphology can also be accessed while keeping the temperature above LCST by introducing complementary DNA strands with single stranded overhang regions. These results demonstrate the multidimensional shape changing capability of DNA-*b*-PNIPAM-*b*-PMA enabled by the dual-responsive property.

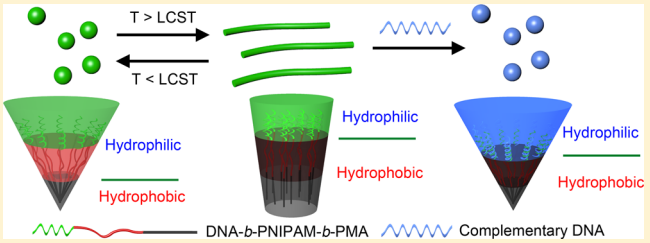

INTRODUCTION

Dynamic nanostructures that can undergo structural changes in response to external stimuli or environmental changes are of great interest for a range of applications such as drug delivery,[1,2] catalysis,[3] self-healing materials,[4] responsive textiles,[5] and optoelectronic devices.[6] Such smart materials have been constructed to operate under various types of stimuli (e.g., temperature,[7−12] pH,[10,13] light,[14] redox potential,[10,15] DNA,[16] and enzymes[17,18]).

Poly(*N*-isopropylacrylamide) (PNIPAM) is a widely used thermoresponsive polymer due to its reversible and sharp phase transition. PNIPAM is hydrophilic below lower critical solution temperature (LCST) due to hydrogen bonding with water and undergo entropy-driven phase transition to hydrophobic polymer at LCST.[19] The LCST of PNIPAM typically ranges from 30 to 35 °C and can be adjusted close to the physiological temperature,[20] which makes it a suitable component for developing smart responsive materials for various applications. PNIPAM-grafted nanoparticles have been synthesized to create new materials with thermoresponsive capabilities such as temperature-sensitive smart windows,[21] thermally induced magnetic separation,[22] and temperature-triggered on−off molecular recognition properties.[7] Researchers have also demonstrated that PNIPAM block copolymers can be designed to undergo thermally induced reversible micelle-to-vesicle morphology changes.[8,9,23−25]

DNA block copolymers, an oligonucleotide covalently attached to a hydrophobic polymer, have been demonstrated to be a versatile building block for making programmable nanostructures.[26] They can self-assemble into various types of nanostructures with recognition properties of DNA and are capable of programmable morphological changes in response to the addition of enzymes and DNA.[18] In addition, they possess a number of interesting properties such as high binding capacity,[27,28] efficient cellular uptake,[29,30] and resistance to nuclease digestion,[31] and have been demonstrated to be efficient delivery vehicles for anticancer drugs[32] and therapeutic nucleic acids.[33] In most previous studies, however, DNA strands were coupled to prototypical nonresponsive polymers such as polystyrene,[34] poly(propylene) oxide,[29,35] and norborene-based polymers,[31,33] where the role of the hydrophobic polymer was limited to granting amphiphilicity to the polymer for self-assembly. Recently, there have been a few reports on DNA-coupled functional polymers.[11,12,36] For example, Maeda and co-workers synthesized DNA-*b*-PNIPAM and studied their temperature-induced aggregation behavior.[11] O'Reilly and co-workers

Received: August 2, 2016
Published: October 28, 2016

DOI: 10.1021/jacs.6b07985
J. Am. Chem. Soc. 2016, 138, 14941−14947

have demonstrated the formation of polymer-decorated DNA polyhedron with DNA-*b*-PNIPAM.[12]

Herein, we synthesized dual-responsive DNA di- and triblock copolymers of DNA-*b*-PNIPAM and DNA-*b*-PNIPAM-*b*-poly(methyl acrylate) (DNA-*b*-PNIPAM-*b*-PMA) with distinct temperature-dependent self-assembly behaviors. We demonstrate that the dual-functional DNA/PNIPAM block copolymers can undergo dynamic and multidimensional morphological transitions with controllable temperature windows among molecular DNA, spherical micelles, and cylindrical micelles through the combination of thermal trigger and DNA binding.

RESULTS AND DISCUSSION

Synthesis and Characterization of DNA Diblock and Triblock Copolymers. Thermosensitive DNA diblock and triblock copolymers were synthesized by coupling carboxylic acid terminated PNIPAM or PNIPAM-*b*-PMA with amine terminated oligonucleotides (Scheme 1). First, carboxylic acid terminated PNIPAM was synthesized by the RAFT polymerization using a chain transfer agent (CTA) containing a carboxylic acid group (Scheme 1a). Two different batches of PNIPAM with different molecular weights [i.e., M_n = 11500 g/mol (repeat unit (n) = 98), 21100 g/mol (n = 183)] were prepared and used for the syntheses of DNA block copolymers. The LCST values of $PNIPAM_{98}$ and $PNIPAM_{183}$ were measured to be 32.5 and 31.1 °C, respectively (Figure S1). These results are consistent with earlier reports showing molecular-weight-dependent LCST.[37] For the synthesis of triblock copolymers, $PNIPAM_{183}$ was used as a macro-CTA for the polymerization of the second block, PMA, to prepare PNIPAM-*b*-PMA (Scheme 1a). The synthesized PNIPAM and PNIPAM-*b*-PMA were characterized by gel permeation chromatography (GPC) and nuclear magnetic resonance (NMR) (Figures S2 and S3 and Table S1).

DNA block copolymers were synthesized by coupling carboxylic acid terminated polymers (i.e., PNIPAM, PNIPAM-*b*-PMA) to amine-modified oligonucleotides (DNA1) that are attached on controlled pore glass (CPG) beads (Scheme 1b). The DNA strands were labeled with fluorescein (FAM) at the 3′ end for DNA binding studies. After 24 h of coupling reaction, unreacted polymers were removed by rinsing the CPG beads with copious amounts (~10 × 5 mL) of DMF, chloroform, and acetone. Then, DNA block copolymers and uncoupled DNA were cleaved from the beads using concentrated ammonium hydroxide. Synthesized DNA1(FAM)-*b*-PNIPAM and DNA1(FAM)-*b*-PNIPAM-*b*-PMA were purified from uncoupled DNA1(FAM) by gel electrophoresis (Figure S4). More detailed experimental procedures and DNA sequences (Table S2) are provided in Supporting Information.

Scheme 1. (a) Synthetic Scheme of PNIPAM and PNIPAM-*b*-PMA and (b) Synthetic Scheme of DNA Block Copolymers (DNA1 Sequence: 3′-FAM-AACTTATAACTATTCCTA-A_3-5′)

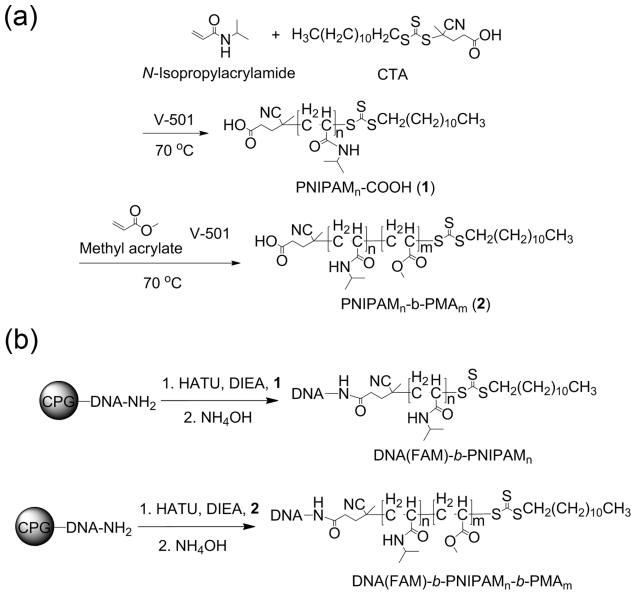

As expected, DNA1(FAM)-*b*-PNIPAM-*b*-PMA formed micelles in water while DNA1(FAM)-*b*-PNIPAM dissolved as isolated polymers in water at room temperature. The DNA binding capabilities of DNA1(FAM)-*b*-PNIPAM strands and DNA1(FAM)-*b*-PNIPAM-*b*-PMA micelles were confirmed by measuring fluorescence resonance energy transfer (FRET) between FAM-labeled DNA block copolymers and Cy3-labeled complementary DNA strands (DNA1′(Cy3)) (Figure S5). DNA block copolymers (i.e., DNA1(FAM)-*b*-PNIPAM and DNA1(FAM)-*b*-PNIPAM-*b*-PMA micelles) showed slightly higher melting temperatures (T_m) and sharper melting transitions than DNA1(FAM) (Figure S5) as expected due to the cooperative binding effect of densely packed DNA strands in polymer micelles.[38] The melting temperature of DNA block copolymers can be controlled by varying the GC content or DNA length. However, high GC content in DNA can lead to micelle aggregation via G-quadruplex formation.[39] Such factors should be considered in designing DNA sequences for DNA block copolymers.

Thermally Induced Self-Assembly of DNA-*b*-PNIPAM. As mentioned above, DNA1(FAM)-*b*-PNIPAM is soluble in water at room temperature. Above LCST, a PNIPAM block becomes hydrophobic, and thus DNA1(FAM)-*b*-PNIPAM becomes amphiphilic, which induces the aggregation of block copolymers into micelles composed of PNIPAM core and DNA corona (Figure 1a). The aggregation number of DNA1(FAM)-*b*-$PNIPAM_{98}$ micelles at 45 °C in water was measured to be 320 by static light scattering (Figure S6). The temperature-triggered self-assembly of DNA1(FAM)-*b*-$PNIPAM_{98}$ was monitored by dynamic light scattering (DLS) measurements in water or in 0.3 M phosphate buffered saline (PBS) buffer (10 mM phosphate, 0.3 M NaCl, pH 7) (Figure 1b). The DLS analyses show the formation of polymer micelles with hydrodynamic diameters of 202 nm (PDI: 0.223) in water and 136 nm (PDI: 0.178) in 0.3 M PBS at 45 °C. The slight size difference in water and PBS buffer can be explained by the charge screening effect of negatively charged DNA strands by cations in 0.3 M PBS. The assembly formation was accompanied by a slight fluorescence intensity reduction due to the self-quenching effect (Figure S7), consistent with the DLS data.

Self-Assembly of DNA-*b*-PNIPAM Micelles and DNA-Modified Gold Nanoparticles. The temperature-dependent aggregation behavior of DNA1(FAM)-*b*-PNIPAM was further probed by the self-assembly of DNA1(FAM)-*b*-PNIPAM and DNA-modified gold nanoparticles (AuNPs) (Figure 2a). For these experiments, AuNPs were coated with DNA1′ (AuNPs-DNA1′), which is complementary to DNA1, by a widely used literature procedure.[40] When AuNPs-DNA1′ was mixed with DNA1(FAM)-*b*-PNIPAM at room temperature (25 °C), no significant changes were observed in the extinction spectra,

DOI: 10.1021/jacs.6b07985
J. Am. Chem. Soc. 2016, 138, 14941−14947

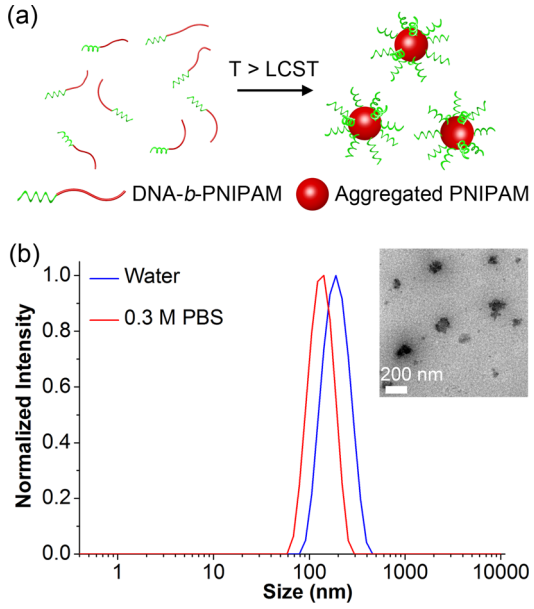

Figure 1. (a) Schematic illustration of heat-induced assembly of DNA-*b*-PNIPAM. (b) DLS analyses of DNA1(FAM)-*b*-PNIPAM$_{98}$ at 45 °C in water and 0.3 M PBS. The inset shows a TEM image of DNA1(FAM)-*b*-PNIPAM$_{98}$ assemblies formed in water. No reliable DLS data were obtained below LCST.

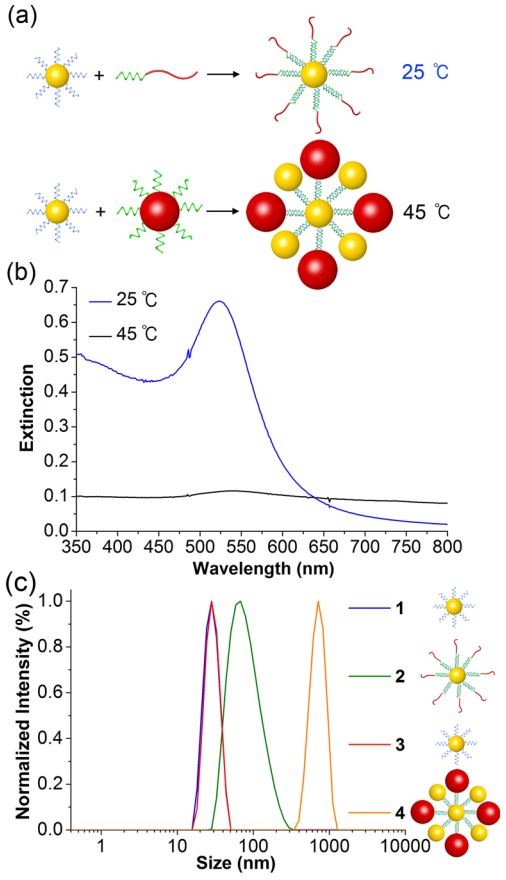

Figure 2. (a) Schematic illustration showing the temperature-dependent aggregation of DNA-*b*-PNIPAM and the DNA-induced binding of DNA-*b*-PNIPAM and DNA-modified nanoparticles at different temperatures. (b) Extinction spectra of AuNPs-DNA1′/DNA1(FAM)-*b*-PNIPAM$_{98}$ mixture in 0.3 PBS at two different temperatures. (c) DLS analyses of AuNPs-DNA1′ (**1** and **3**) and AuNPs-DNA1′ mixed with DNA1(FAM)-*b*-PNIPAM$_{98}$ (**2** and **4**) in 0.3 M PBS at 25 °C (**1** and **2**) and 45 °C (**3** and **4**).

indicating no nanoparticle network formation (Figure 2b). On the other hand, when the two components were mixed at a temperature above LCST, nanoparticles and DNA1(FAM)-*b*-PNIPAM micelles are linked together into macroscopic aggregates through DNA hybridization, as evidenced by the red-shift and broadening of surface plasmon resonance (SPR) band[38] (Figure 2b). Zeta potential measurements at 45 °C showed that both AuNPs-DNA1′ (−28.2 ± 0.2 mV) and DNA1(FAM)-*b*-PNIPAM$_{98}$ (−5.1 ± 0.2 mV) are negatively charged, excluding the possibility of aggregate formation by the electrostatic attraction.

DLS data are consistent with the observation (Figure 2c). At room temperature, the addition of DNA1(FAM)-*b*-PNIPAM to AuNPs-DNA1′ resulted in a slight increase of particle size from 29 to 86 nm due to the binding of DNA1(FAM)-*b*-PNIPAM to AuNPs-DNA1′ (Figure 2c, **2**). At 45 °C, DLS signal shifted to the micrometer range, indicating the network formation between polymer micelles and gold nanoparticles (Figure 2c, **4**). These results confirm the temperature-triggered switch between the molecular and aggregate states of DNA-*b*-PNIPAM.

Thermoresponsive Nanoparticles. The hybridization of DNA1(FAM)-*b*-PNIPAM to AuNPs-DNA1′ results in a new type of thermoresponsive particles composed of AuNP core/DNA bridge/PNIPAM corona (AuNP/DNA/PNIPAM), as illustrated in Figure 2a and Scheme 2. As both DNA and PNIPAM are capable of temperature-induced conformational changes, the aggregation of nanoparticles can be controlled by both DNA bridges and PNIPAM corona (Scheme 2).

The temperature-dependent behavior of the layered AuNP/DNA/PNIPAM particles was examined by extinction and transmission electron microscopy (TEM) measurements (Figure 3a). The optical signature of AuNPs allows us to easily measure the LCST of PNIPAM and melting temperature of DNA, as the aggregation of AuNPs induces a red-shift and broadening of SPR bands.[38] Due to the dual-responsive nature of AuNP/DNA/PNIPAM particles, they show unique well-shape transition curves with temperature; the spectra used to construct the transition curves are given in Figure S8. The AuNP/DNA/PNIPAM particles are well-dispersed in buffer at room temperature as mentioned above and show a well-defined SPR band at 524 nm. With the increase of temperature over LCST of PNIPAM, AuNP/DNA/PNIPAM particles are aggregated into a massive network of nanoparticles and polymers due to the transition of PNIPAM corona from hydrophilic state to hydrophobic state, as evidenced by the broadening of the SPR band. Note that the LCST of PNIPAM increases from 32.5 to 38.3 °C with the attachment of DNA (Figure 3a). This observation is consistent with previous reports showing that the LCST changes with the attachment of hydrophilic molecules.[10,37,41] The temperature-induced assembly is reversible, and the nanoparticle/polymer aggregates can be disassembled by lowering the temperature below LCST.

Furthermore, unlike simple PNIPAM-modified nanoparticles,[21,22,42] these aggregates were redispersed into DNA-modified nanoparticles and polymer micelles by increasing the temperature above the DNA melting temperature (Scheme 2, 65.6 °C), as evidenced by the SPR band at 522 nm. The nanoparticle disaggregation due to DNA melting at high temperature shows sharp transitions (Figure 3, Figure S9–S10), as expected for high density DNA bridges.[38] TEM images

DOI: 10.1021/jacs.6b07985
J. Am. Chem. Soc. 2016, 138, 14941−14947

Scheme 2. Schematic Illustration Showing the Temperature-Dependent Dispersion and Aggregation Behavior of AuNP/DNA/PNIPAM Particles

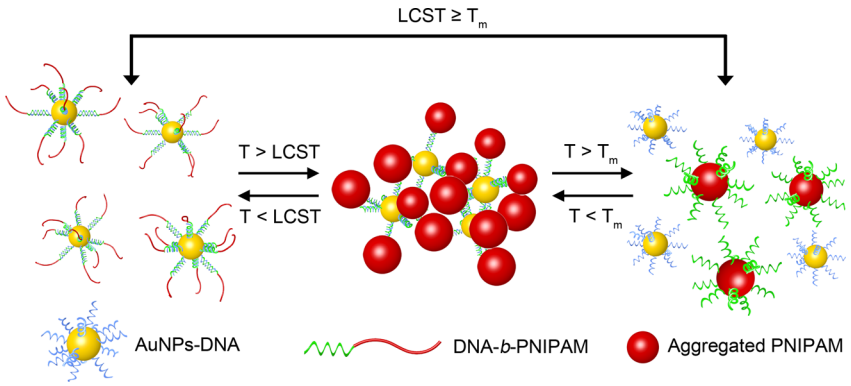

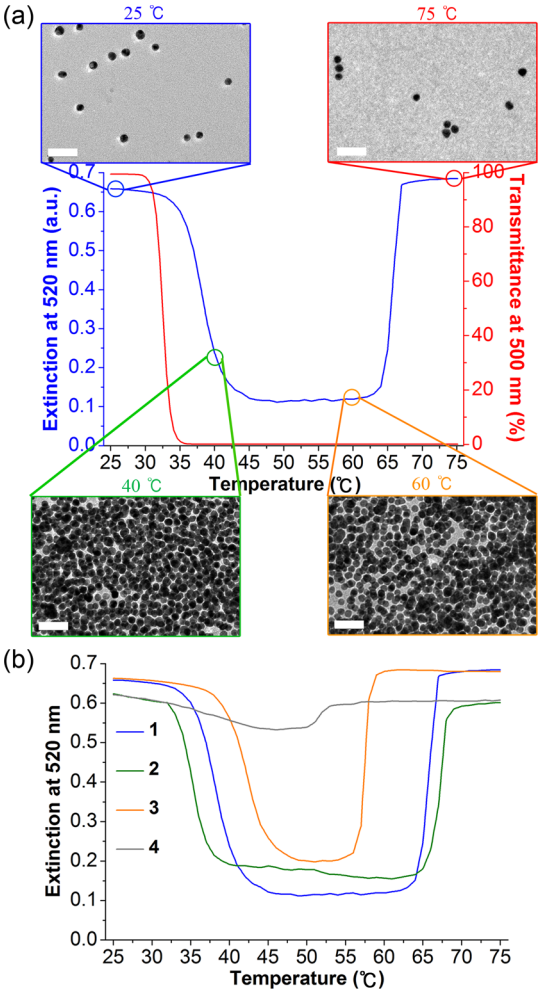

Figure 3. (a) Temperature-dependent extinction at 520 nm and TEM images (scale bars: 50 nm) of AuNP/DNA/PNIPAM particles formed by the hybridization of DNA1(FAM)-*b*-$PNIPAM_{98}$ and AuNPs-DNA1′ in 0.3 M PBS (blue line). The concentrations of AuNPs-DNA and DNA-*b*-PNIPAM were 6 and 240 nM, respectively. Temperature-dependent transmission of $PNIPAM_{98}$ is given for comparison (red line). (b) Temperature-dependent extinction profiles of AuNPs-DNA1′ hybridized with DNA1(FAM)-*b*-$PNIPAM_{98}$ in 0.3 M PBS (**1**, blue line), 0.1 M PBS (**3**, violet line), or 50 mM PBS (**4**, gray line). The green line is the same curve obtained for DNA1(FAM)-*b*-$PNIPAM_{183}$ in 0.3 M PBS (**2**, green line). The concentrations of AuNPs-DNA and DNA-*b*-PNIPAM were set as 6 and 240 nM, respectively.

obtained at different temperatures are consistent with the optical signatures (Figure 3a).

The ability to regulate the transition temperature is important for wide applications of thermosensitive nanomaterials.[42,43] As the DNA melting temperature can be easily controlled over a broad temperature range by varying the length of complementary sequence or by adjusting salt concentration, the second transition temperature for disaggregation can be readily controlled in this dual-responsive system. The data presented in Figure 3b demonstrate such capability; DNA melting temperature decreases by 8.1 °C with decreasing the salt concentration from 0.3 M PBS to 0.1 M PBS. The salt concentration also affects LCST and the aggregation temperature; because ions in PBS buffer attenuate the hydrogen bonding between water and amide group of PNIPAM,[44,45] the reduction of salt concentration from 0.3 to 0.1 M increases the LCST from 38.3 to 42.0 °C (Figure 3b).[44−46] The LCST of PNIPAM can also be controlled by varying the molecular weight of PNIPAM;[37,47] increasing the polymer length from $PNIPAM_{98}$ to $PNIPAM_{183}$ decreased the LCST from 38.3 to 35.2 °C and slightly increased the DNA melting temperature from 65.6 to 67.1 °C in 0.3 M PBS (Figure 3b). These results demonstrate that while the change in one block slightly affects the properties of the other block, the transition temperatures of both blocks (i.e., LCST and T_m) in DNA-*b*-PNIPAM can be independently addressed, and thus, the temperature range for the aggregation window can be readily adjusted for specific needs. Furthermore, the middle aggregate state can be bypassed depending on the strand design and conditions (Scheme 2). When the salt concentration was decreased further to 50 mM PBS, T_m becomes comparable to LCST, and Au/DNA/PNIPAM particles show only shallow dipping in temperature-dependent extinction data (Figure 3b, Figure S11). This data indicate that AuNP/DNA/PNIPAM particles undergo a direct transition to the high temperature state without significant macroscopic aggregation of nanoparticles in the process. We envision that such capability can be useful for protected drug and gene delivery applications.

Dual-Responsive Shape Transformation of DNA Triblock Copolymer Assemblies. The dual-responsive DNA triblock copolymers are capable of morphology changes with temperature cues as well as DNA's molecular recognition properties (Scheme 3). To demonstrate such capability, DNA-*b*-PNIPAM-*b*-PMA strands were first assembled into small micelles at room temperature (green spheres in Scheme 3). TEM images revealed the formation of well-defined spherical micelles (Figure 4a). The hydrodynamic diameter of DNA1(FAM)-*b*-PNI-

DOI: 10.1021/jacs.6b07985
J. Am. Chem. Soc. 2016, 138, 14941−14947

Scheme 3. Morphology Changes of DNA-*b*-PNIPAM-*b*-PMA Micelles in Response to the Temperature Changes and Hybridization with Complementary DNA

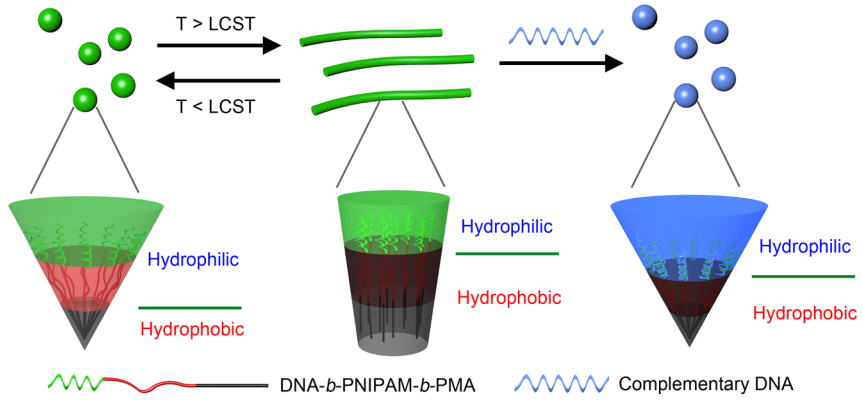

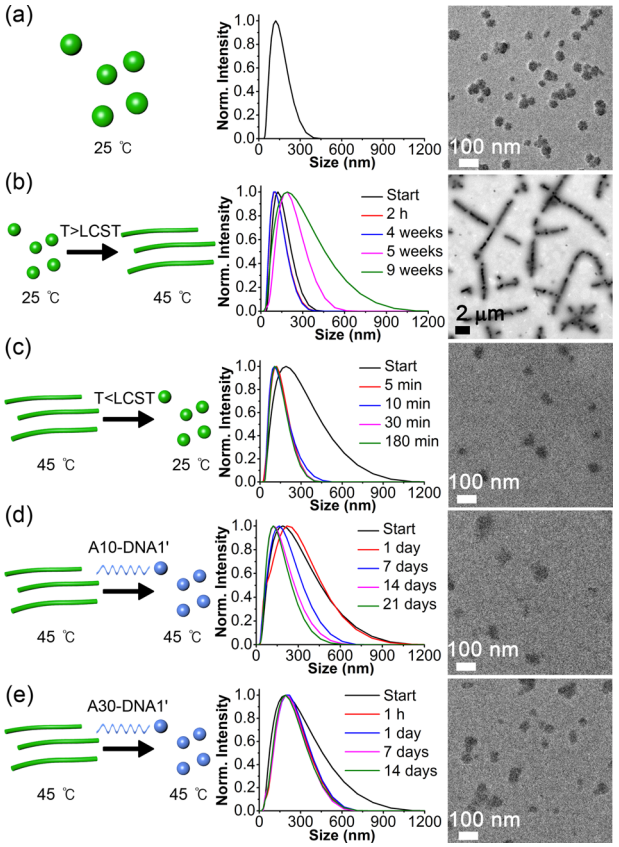

Figure 4. Dual-responsive morphology change and recovery of DNA1(FAM)-*b*-PNIPAM$_{183}$-*b*-PMA$_{118}$ micelles detected by DLS and TEM. (a) DNA1(FAM)-*b*-PNIPAM$_{183}$-*b*-PMA$_{118}$ micelles at 25 °C. (b) Thermoactivated morphology change of DNA1(FAM)-*b*-PNIPAM$_{183}$-*b*-PMA$_{118}$ micelles at 45 °C. (c) Morphology recovery of DNA1(FAM)-*b*-PNIPAM$_{183}$-*b*-PMA$_{118}$ micelles from cylinders to spheres by decreasing temperature. (d, e) Morphology recovery of DNA1-(FAM)-*b*-PNIPAM$_{183}$-*b*-PMA$_{118}$ micelles by adding DNA1′ having overhang sequence as A$_{10}$ and A$_{30}$ at 45 °C. These hydrodynamic diameters, detected by DLS, are the average of three measurements except 5, 10, 30, and 180 min data in part c. The TEM data in parts b–e are from 9 weeks, 180 min, 21 days, and 14 days. All experiments were carried out in 5 mM Tris-HCl buffer with 5 mM $MgCl_2$.

PAM$_{183}$-*b*-PMA$_{118}$ micelles was measured to be 135 nm (PDI: 0.173) by DLS (Figure 4a). At room temperature, the central block of PNIPAM is hydrophilic, and the hydrophilic block (DNA and PNIPAM) volume is significantly larger than the hydrophobic block (PMA) volume. Therefore, small micelles with high interface curvature are formed at room temperature (Figure 4a). When the temperature is increased above LCST, the volume fraction of hydrophobic part is increased as PNIPAM becomes hydrophobic, as illustrated in Scheme 3. This relative hydrophobic volume change can induce morphology changes to assemblies with smaller interfacial curvature such as cylindrical micelles or vesicles.

The temperature-induced morphology change of DNA1-(FAM)-*b*-PNIPAM$_{183}$-*b*-PMA$_{118}$ was first monitored by DLS over time in buffer and water, respectively (Figure 5). As the temperature increased from 25 to 45 °C, the hydrodynamic diameter initially decreased from 135 to 118 nm (PDI: 0.181) in buffer and from 136 to 122 nm (PDI: 0.153) in water within 1 h,

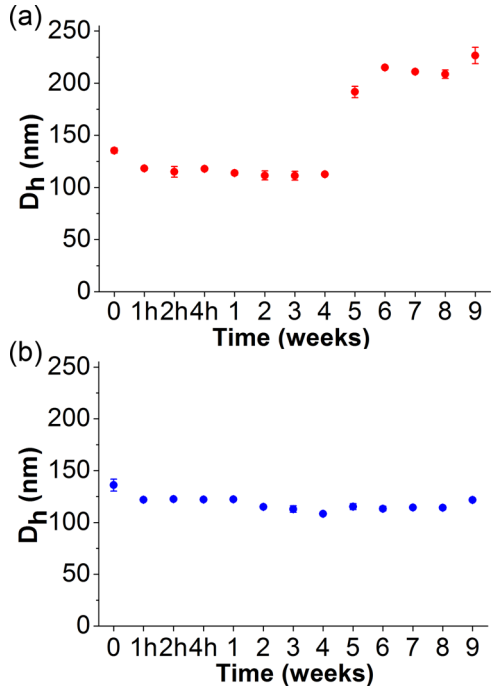

Figure 5. Time-dependent hydrodynamic diameters (D_h) of DNA1-(FAM)-*b*-PNIPAM$_{183}$-*b*-PMA$_{118}$ micelles at 45 °C in (a) 5 mM Tris-HCl buffer with 5 mM $MgCl_2$ and 0.01% sodium azide (pH = 7) and (b) water with 0.01% sodium azide. These hydrodynamic diameters are the average of three measurements.

DOI: 10.1021/jacs.6b07985
J. Am. Chem. Soc. 2016, 138, 14941–14947

respectively. This initial size reduction is attributed to the dehydration of PNIPAM above LCST. Eventually, the hydrodynamic diameter began to increase after a few weeks of incubation at 45 °C in buffer (Figure 5a). There was no significant change in DLS data when the micelles were kept in water at the same temperature (45 °C) (Figure 5b), presumably due to the highly negatively charged DNA backbone. In buffer, cations screen the negative charge on DNA and reduce the relative hydrophilic block volume and also the repulsive interactions between micelles, which allows for the observed morphology changes. TEM imaging of polymer assemblies incubated at 45 °C showed the formation of cylindrical micelles, consistent with the DLS data (Figure 4b). The morphology change is reversible, and a majority of cylinders were broken into small micelles when the temperature was reduced below LCST (Figure 4c, Figure S12). The size of micelles was measured to be 125 nm (PDI: 0.290) by DLS, which is similar to the size of the initial micelles (135 nm). The cylinder-to-micelle transition was relatively fast, and the morphology change occurred within 5 min of temperature reduction. The micelle-to-cylinder transition takes a much longer time than the cylinder-to-micelle transition, as it requires the collision and fusion of many spherical micelles.[24]

Cylinder-to-micelle transition can also be induced while keeping the temperature above LCST by using the molecular recognition properties of DNA (Figure 4d,e). In this experiment, DNA strands composed of DNA1′ and A_{10} or A_{30} overhangs (A_{10}-DNA1′ or A_{30}-DNA1′) act as a "stimulus" DNA that triggers morphology changes. Since the binding of "stimulus" DNA (Figure S13) increases the hydrophilic block volume (Scheme 3), the DNA binding events can induce cylinder-to-sphere morphology changes (Figure 4d,e). TEM images showed that a majority of cylinders were broken into micelles with the addition of DNA (Figure S12). Time-dependent DLS measurements showed that the morphology recovery from cylinder to sphere was completed in a few weeks after the addition of A_{10}-DNA1′ (Figure 4e). The recovery time was controllable by adjusting the length of the DNA overhang. With A_{30}-DNA1′, the morphology change was completed within hours of DNA addition (Figure 4e). The hydrodynamic diameters of recovered micelles were 144 nm (PDI: 0.260) for A_{10}-DNA1′ (21 days) and 197 nm (PDI: 0.248) for A_{30}-DNA1′ (14 days), respectively, which were larger than that for the initial micelles (135 nm, Figure 4a) due to the volume taken up by the DNA overhang corona (Figure 4d,e). Note that the temperature-induced cylinder-to-micelle morphology change through the conformational changes in the PNIPAM domain is much faster than DNA-induced morphology changes. These results indicate that the kinetics of morphology change is controllable through the choice of stimuli.

CONCLUSION

Here, we synthesized dual-responsive DNA di- and triblock copolymers by coupling a widely used thermoresponsive polymer, PNIPAM, and DNA (i.e., DNA-*b*-PNIPAM and DNA-*b*-PNIPAM-*b*-PMA). DNA-*b*-PNIPAM possesses thermoresponsive properties of PNIPAM as well as molecular recognition properties of DNA. They are soluble in water at room temperature and undergo temperature-induced micellization at LCST into spherical assemblies with densely packed DNA corona. The hybridization of DNA-*b*-PNIPAM and DNA-modified AuNPs at room temperature yields thermoresponsive nanoparticles composed of AuNP core, DNA bridge, and PNIPAM corona. They show unique temperature-induced aggregation and dispersion behavior and undergo two thermally induced transitions at LCST and T_m among three different states (i.e., low temperature dispersion state, middle temperature aggregation state, and high temperature dispersion state). Each transition temperature can be regulated by adjusting the length of PNIPAM, DNA sequences, and solution conditions with the capability of bypassing the middle aggregation state. Triblock copolymer of DNA-*b*-PNIPAM-*b*-PMA was synthesized to form dual-responsive DNA micelles at room temperature. They are designed to undergo multidimensional nanoscale morphological transitions in response to both temperature and DNA. When dispersed in buffer at room temperature, they form high curvature spherical micelles composed of PMA core, thermoresponsive PNIPAM layer, and DNA corona. Above LCST, they slowly transform into cylindrical micelles as the middle PNIPAM block becomes hydrophobic. This shape transformation is reversible. Fast cylinder-to-sphere morphological transition occurs by reducing the temperature below LCST. The same morphology change can occur while keeping the temperature above LCST by taking advantage of DNA's molecular recognition properties. Such DNA block copolymers can be synthesized with other thermoresponsive polymers such as more biocompatible polymers (e.g., random *N*,*N*-diethylacrylamide/*N*,*N*-dimethylacrylamide copolymers[48]) and polymers exhibiting the upper critical solution temperature character (e.g., poly(3-[*N*-(3-methacrylamido-propyl)-*N*,*N*-dimethyl]-ammonio propionate sulfonate)[49]). The multidimensional shape changing capabilities and controllable transition temperatures of dual-responsive DNA block copolymers should be useful for the fabrication of dynamic nanostructures and designing smart drug and gene delivery systems.

ASSOCIATED CONTENT

Supporting Information

The Supporting Information is available free of charge on the ACS Publications website at DOI: 10.1021/jacs.6b07985.

Materials and instrumentation, synthesis and characterization details, detailed procedures for self-assembly, additional characterization data, thermal denaturation curves and TEM images of polymer assemblies, and selected UV−vis spectra used to construct temperature-dependent optical data (PDF)

AUTHOR INFORMATION

Corresponding Author

*sojungpark@ewha.ac.kr

Notes

The authors declare no competing financial interest.

ACKNOWLEDGMENTS

This work was supported by the National Research Foundation of Korea (NRF) grant funded by the Korea government (MSIP) (NRF-2015R1A2A2A01003528).

REFERENCES

(1) Mura, S.; Nicolas, J.; Couvreur, P. *Nat. Mater.* **2013**, *12*, 991−1003.
(2) Blum, A. P.; Kammeyer, J. K.; Rush, A. M.; Callmann, C. E.; Hahn, M. E.; Gianneschi, N. C. *J. Am. Chem. Soc.* **2015**, *137*, 2140−2154.
(3) Vriezema, D. M.; Comellas Aragonès, M.; Elemans, J. A.; Cornelissen, J. J.; Rowan, A. E.; Nolte, R. J. *Chem. Rev.* **2005**, *105*, 1445−1490.

DOI: 10.1021/jacs.6b07985
J. Am. Chem. Soc. 2016, 138, 14941−14947

(4) Shchukin, D. G.; Möhwald, H. *Small* **2007**, *3*, 926−943.
(5) Crespy, D.; Rossi, R. M. *Polym. Int.* **2007**, *56*, 1461−1468.
(6) Dong, Y.; Xu, B.; Zhang, J.; Tan, X.; Wang, L.; Chen, J.; Lv, H.; Wen, S.; Li, B.; Ye, L.; et al. *Angew. Chem., Int. Ed.* **2012**, *51*, 10782−10785.
(7) Zhang, K.; Zhu, X.; Jia, F.; Auyeung, E.; Mirkin, C. A. *J. Am. Chem. Soc.* **2013**, *135*, 14102−14105.
(8) Cai, Y.; Aubrecht, K. B.; Grubbs, R. B. *J. Am. Chem. Soc.* **2011**, *133*, 1058−1065.
(9) Moughton, A. O.; Patterson, J. P.; O'Reilly, R. K. *Chem. Commun.* **2011**, *47*, 355−357.
(10) Klaikherd, A.; Nagamani, C.; Thayumanavan, S. *J. Am. Chem. Soc.* **2009**, *131*, 4830−4838.
(11) Fujita, M.; Hiramine, H.; Pan, P.; Hikima, T.; Maeda, M. *Langmuir* **2016**, *32*, 1148−1154.
(12) Wilks, T. R.; Bath, J.; de Vries, J. W.; Raymond, J. E.; Herrmann, A.; Turberfield, A. J.; O'Reilly, R. K. *ACS Nano* **2013**, *7*, 8561−8572.
(13) Zhao, Z.; Wang, L.; Liu, Y.; Yang, Z.; He, Y.-M.; Li, Z.; Fan, Q.-H.; Liu, D. *Chem. Commun.* **2012**, *48*, 9753−9755.
(14) Lai, J.; Xu, Y.; Mu, X.; Wu, X.; Li, C.; Zheng, J.; Wu, C.; Chen, J.; Zhao, Y. *Chem. Commun.* **2011**, *47*, 3822−3824.
(15) Yang, Q.; Bai, L.; Zhang, Y.; Zhu, F.; Xu, Y.; Shao, Z.; Shen, Y.-M.; Gong, B. *Macromolecules* **2014**, *47*, 7431−7441.
(16) Estephan, Z. G.; Qian, Z.; Lee, D.; Crocker, J. C.; Park, S.-J. *Nano Lett.* **2013**, *13*, 4449−4455.
(17) Albert, S. K.; Thelu, H. V. P.; Golla, M.; Krishnan, N.; Chaudhary, S.; Varghese, R. *Angew. Chem., Int. Ed.* **2014**, *53*, 8352−8357.
(18) Chien, M. P.; Rush, A. M.; Thompson, M. P.; Gianneschi, N. C. *Angew. Chem., Int. Ed.* **2010**, *49*, 5076−5080.
(19) Okada, Y.; Tanaka, F. *Macromolecules* **2005**, *38*, 4465−4471.
(20) Schild, H. G. *Prog. Polym. Sci.* **1992**, *17*, 163−249.
(21) Zhu, M.-Q.; Wang, L.-Q.; Exarhos, G. J.; Li, A. D. *J. Am. Chem. Soc.* **2004**, *126*, 2656−2657.
(22) Qin, J.; Jo, Y. S.; Muhammed, M. *Angew. Chem.* **2009**, *121*, 7985−7989.
(23) Moughton, A. O.; O'Reilly, R. K. *Chem. Commun.* **2010**, *46*, 1091−1093.
(24) Grubbs, R. B.; Sun, Z. *Chem. Soc. Rev.* **2013**, *42*, 7436−7445.
(25) Sundararaman, A.; Stephan, T.; Grubbs, R. B. *J. Am. Chem. Soc.* **2008**, *130*, 12264−12265.
(26) Kwak, M.; Herrmann, A. *Chem. Soc. Rev.* **2011**, *40*, 5745−5755.
(27) Chen, X. J.; Sanchez-Gaytan, B. L.; Hayik, S. E.; Fryd, M.; Wayland, B. B.; Park, S. J. *Small* **2010**, *6*, 2256−2260.
(28) Luo, Q.; Shi, Z.; Zhang, Y.; Chen, X.-J.; Han, S.-Y.; Baumgart, T.; Chenoweth, D. M.; Park, S.-J. *J. Am. Chem. Soc.* **2016**, *138*, 10157−10162.
(29) Alemdaroglu, F. E.; Alemdaroglu, N. C.; Langguth, P.; Herrmann, A. *Macromol. Rapid Commun.* **2008**, *29*, 326−329.
(30) Liu, H.; Zhu, Z.; Kang, H.; Wu, Y.; Sefan, K.; Tan, W. *Chem. - Eur. J.* **2010**, *16*, 3791−3797.
(31) Rush, A. M.; Thompson, M. P.; Tatro, E. T.; Gianneschi, N. C. *ACS Nano* **2013**, *7*, 1379−1387.
(32) Alemdaroglu, F. E.; Alemdaroglu, N. C.; Langguth, P.; Herrmann, A. *Adv. Mater.* **2008**, *20*, 899−902.
(33) Rush, A. M.; Nelles, D. A.; Blum, A. P.; Barnhill, S. A.; Tatro, E. T.; Yeo, G. W.; Gianneschi, N. C. *J. Am. Chem. Soc.* **2014**, *136*, 7615−7618.
(34) Li, Z.; Zhang, Y.; Fullhart, P.; Mirkin, C. A. *Nano Lett.* **2004**, *4*, 1055−1058.
(35) Alemdaroglu, F. E.; Ding, K.; Berger, R.; Herrmann, A. *Angew. Chem., Int. Ed.* **2006**, *45*, 4206−4210.
(36) Kamps, A. C.; Cativo, M. H. M.; Chen, X.-J.; Park, S.-J. *Macromolecules* **2014**, *47*, 3720−3726.
(37) Xia, Y.; Yin, X.; Burke, N. A.; Stöver, H. D. *Macromolecules* **2005**, *38*, 5937−5943.
(38) Cutler, J. I.; Auyeung, E.; Mirkin, C. A. *J. Am. Chem. Soc.* **2012**, *134*, 1376−1391.
(39) Hurst, S. J.; Hill, H. D.; Macfarlane, R. J.; Wu, J.; Dravid, V. P.; Mirkin, C. A. *Small* **2009**, *5*, 2156−2161.
(40) Storhoff, J. J.; Elghanian, R.; Mucic, R. C.; Mirkin, C. A.; Letsinger, R. L. *J. Am. Chem. Soc.* **1998**, *120*, 1959−1964.
(41) Xia, Y.; Burke, N. A.; Stöver, H. D. *Macromolecules* **2006**, *39*, 2275−2283.
(42) Lemieux, V.; Adams, P. H. H.; van Hest, J. C. *Chem. Commun.* **2010**, *46*, 3071−3073.
(43) Shen, Y.; Kuang, M.; Shen, Z.; Nieberle, J.; Duan, H.; Frey, H. *Angew. Chem., Int. Ed.* **2008**, *47*, 2227−2230.
(44) Hocine, S.; Li, M.-H. *Soft Matter* **2013**, *9*, 5839−5861.
(45) Zhang, Y.; Furyk, S.; Bergbreiter, D. E.; Cremer, P. S. *J. Am. Chem. Soc.* **2005**, *127*, 14505−14510.
(46) Zhang, Y.; Furyk, S.; Sagle, L. B.; Cho, Y.; Bergbreiter, D. E.; Cremer, P. S. *J. Phys. Chem. C* **2007**, *111*, 8916−8924.
(47) Lessard, D.; Ousalem, M.; Zhu, X. *Can. J. Chem.* **2001**, *79*, 1870−1874.
(48) Lu, X.; Sun, M.; Barron, A. E. *J. Colloid Interface Sci.* **2011**, *357*, 345−353.
(49) Dimitrov, I.; Trzebicka, B.; Müller, A. H.; Dworak, A.; Tsvetanov, C. B. *Prog. Polym. Sci.* **2007**, *32*, 1275−1343.

DOI: 10.1021/jacs.6b07985
J. Am. Chem. Soc. 2016, 138, 14941−14947